Int. J. Multiphase Flow Vol. 10, No. 6, pp. 697–710, 1984
Printed in the U.S.A.

0301-9322/84 $3.00 + .00
Pergamon/Elsevier

PREDICTION OF THE PARTICLE-LADEN JET WITH A TWO-EQUATION TURBULENCE MODEL

S. ELGHOBASHI, T. ABOU-ARAB, M. RIZK and A. MOSTAFA
Mechanical Engineering Department, University of California, Irvine, CA 92717, U.S.A.

(*Received* 25 *November* 1983; *in revised form* 7 *February* 1984)

Abstract—A two-equation turbulence model for two-phase flows has recently been proposed by Elghobashi & Abou-Arab (1983). They derived the exact equations of the kinetic energy of turbulence and the rate of dissipation of that energy, and modeled the turbulent correlations, resulting from time-averaging, up to third order. In order to validate the proposed model, a turbulent axisymmetric gaseous jet laden with spherical uniform-size solid particles is studied here. The predictions of the mean flow properties of the two-phases and the turbulence kinetic energy and shear stress of the carrier phase show good agreement with the experimental data.

1. INTRODUCTION

Particle-laden turbulent jets occur in many engineering applications. Pulverised-coal combustors, diesel-engine sprays, aerosols and rocket plumes are some examples. In order to enhance the understanding of the interaction between the dispersed phase and the carrier fluid in these jets parallel experimental and theoretical studies are needed. The need for this coordinated effort stems from the fact that until very recently it was impossible to find in the literature a well-documented experimental study of a two-phase turbulent jet. In fact until a year ago the only two available experimental studies of two-phase turbulent jets (Hetsroni & Sokolov 1971; Popper *et al.* 1974) did not report the radial profiles of the main dependent variables at the nozzle exit. This information is essential for accurately predicting such flow as it is known that the dependence of the downstream flow upon the nozzle conditions persists for at least 50 nozzle diameters (Barker 1973). The recent experiment of Modarress *et al.* (1982, 1983), which was performed in parallel with the present work, provided a much needed data to help understand the behavior of two-phase turbulent jets and validate the theoretical models. Elghobashi & Abou-Arab (1983) reviewed existing turbulence models for two-phase flows and indicated that these models are based on ad hoc modifications of single-phase turbulence models. They developed a two-equation turbulence model for incompressible dilute two-phase flows which undergo no phase changes. The new model was based on rigorously derived transport equations for the two phases. The purpose of this paper is to apply this model to the flow of a turbulent axisymmetric gaseous jet laden with solid, uniform-size particles and compare the predictions with the data of Modarress *et al.* (1982, 1983).

2. THE FLOW CONSIDERED

Figure 1 shows a sketch of the two-phase turbulent jet considered in this work. Air carrying uniform size glass beads issues vertically downwards from a cylindrical pipe of diameter $D(=0.02\,\text{m})$. The jet is enclosed in a cylindrical container of diameter equal to $30\,D$ to avoid ambient disturbances. Low velocity air stream surrounds the nozzle and extends to the container wall to provide well-defined boundary conditions. Table 1 lists the experimental conditions at $0.1D$ downstream of the pipe exit.

3. MATHEMATICAL MODEL

The governing equations for incompressible turbulent two-phase flows have been derived by Elghobashi & Abou-Arab (1983) by Reynolds decomposition and time averaging the instantaneous equations. Closure of the time-mean equations was achieved

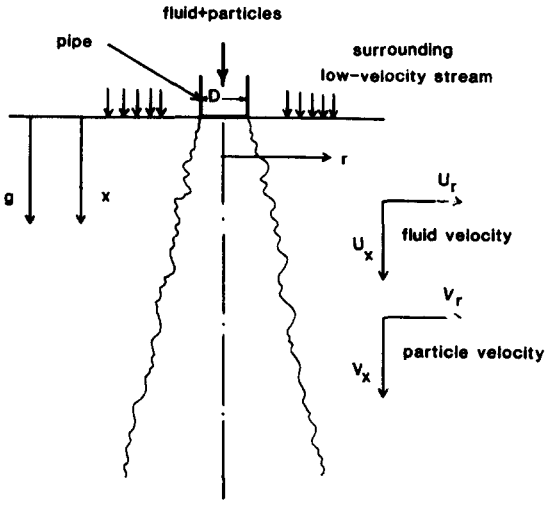

Figure 1. Flow schematic.

by modeling the turbulent correlations up to third order, in the equations of the mean motion, kinetic energy of turbulence and the rate of dissipation of that energy. Assuming the diffusional fluxes in the radial direction to be much greater than those in the axial direction for the flow considered, the governing equations are listed below in the modeled form in cylindrical coordinates.

3.1 *Equations of the mean motion*

The mean motion of each phase is governed by its momentum equations in the axial and radial directions and the conservation of its mass.

The momentum equation of the carrier fluid in the axial (x) direction is:

$$\rho_1\Phi_1U_xU_{x,x}+\rho_1\Phi_1U_rU_{x,r}=-\Phi_1p_{,x}-F\Phi_2(U_x-V_x)+\frac{1}{r}(\rho_1\Phi_1rv_tU_{x,r})_{,r}+c_{m1}\rho_1U_{x,r}\left(\frac{v_t}{\sigma_\Phi}\Phi_{1,r}\right)$$
$$+C_{\phi5}\frac{1}{r}\left(\frac{k}{\epsilon}r\mu_tU_{x,r}\right)_{,r}\left(\frac{v_t}{\sigma_\Phi}\Phi_{1,r}\right)_{,r}+C_{\phi5}\frac{k}{\epsilon}\mu_tU_{x,r}\left(\frac{v_t}{\sigma_\Phi}\Phi_{1,r}\right)_{,rr}. \quad [1]$$

The momentum equation of the solid phase in the axial (x) direction is

$$\rho_2\Phi_2V_xV_{x,x}+\rho_2\Phi_2V_rV_{x,r}=-\Phi_2p_{,x}+F\Phi_2(U_x-V_x)+\frac{1}{r}\left(\rho_2\Phi_2rv_pV_{x,r}\right)_{,r}+C_{m1}\rho_2V_{x,r}$$
$$\times\left(\frac{v_p}{\sigma_\Phi}\Phi_{2,r}\right)+C_{\phi5}\frac{1}{r}\left(\frac{k}{\epsilon}r\mu_pV_{x,r}\right)_{,r}\left(\frac{v_p}{\sigma_\Phi}\Phi_{2,r}\right)_{,r}$$
$$+(\rho_2-\rho_1)g\Phi_2+C_{\phi5}\frac{k}{\epsilon}\mu_pV_{x,r}\left(\frac{v_p}{\sigma_\Phi}\phi_{2,r}\right)_{,rr} \quad [2]$$

where $c_{m1}=0.4$ and $c_{\phi5}=0.1$.

The mean continuity equation of the solid phase is:

$$\rho_2(\Phi_2V_x)_{,x}+\frac{\rho_2}{r}(r\Phi_2V_r)_{,r}-\rho_2\left(\frac{v_p}{\sigma_\Phi}\Phi_{2,x}\right)_{,x}-\frac{\rho_2}{r}\left(r\frac{v_p}{\sigma_\Phi}\Phi_{2,r}\right)_{,r}=0. \quad [3]$$

Table 1. Experimental flow conditions at 0.1D downstream of pipe exit

Gas-Phase (Air):	Case 1	Case 2	Case 3
Centerline velocity, $U_{x,c}$ (m/s)	12.6	12.6	13.4
Exponent, n, of power law velocity Profile $U_x/U_{x,c} = (1-(2r/D))^{1}/n$	<---------- 6.6---------->		
Turbulence Intensity $(u_x/U_{x,c})$	<--------(0.04 + 0.1 r/D)-------->		
Density, ρ_1 (Kg/m^3)	<---------- 1.178---------->		
Mass flow rate $\dot{m}_1$ (Kg/s)	3.76×10^{-3}	3.76×10^{-3}	4×10^{-3}
Reynolds number $R_e = (4\dot{m}_1/\pi\mu_1 D)$	13300	13300	14100
Uniform mean velocity of surrounding stream, $U_{x,s}$ (m/s)	<---------- 0.05---------->		
Intensity of turbulence in surrounding $(u_{x,s}/U_{x,s})$	<---------- 0.1---------->		
Particle diameter (microns)	50	50	200
Particle density, ρ_2 (Kg/m^3)	<---------- 2990---------->		
Centerline velocity, $V_{x,c}$ (m/s)	12.4	12.4	10.2
Exponent, n, of power law velocity profile	<---------- 27.6---------->		
Mass flow rate $\dot{m}_2$ (Kg/s)	1.2×10^{-3}	3.2×10^{-3}	3.2×10^{-3}
Ratio of mass flow rates $\phi_o = \dot{m}_2/\dot{m}_1$	0.32	0.85	0.8
Ratio of volumetric fractions = $\phi_2/\phi_1 = (\dot{m}_2/\dot{m}_1)(\rho_1 U_{x,av.}/\rho_2 V_{x,av.})$	1.1×10^{-4}	2.9×10^{-4}	3.52×10^{-4}

The mean global continuity equation is:

$$\Phi_1 + \Phi_2 = 1. \qquad [4]$$

In the above equations the comma-suffix notation indicates differentiation with respect to the spatial coordinates x and r. U and V are respectively the mean velocities of the carrier fluid and dispersed phase. The subscripts 1 and 2 denote respectively the carrier fluid and the dispersed phase. ρ is the material density, Φ the mean volume fraction, p the mean pressure, μ_t the eddy viscosity of the fluid, ν_p the kinematic eddy viscosity of the dispersed phase, ν_t the kinematic eddy viscosity of the fluid, σ_Φ the turbulent Schmidt number of the volume fraction (its numerical value is given in Table 2) and g is the acceleration due to gravity.

The two terms on the l.h.s. of [1] represent the inertia force per unit volume due to fluid acceleration in the x and r directions. The first term on the r.h.s. is the force due to pressure gradient and the second is the drag force due to the slip between the two phases. The third term represents the turbulent diffusion of the fluid's momentum. The fourth term models the correlations $\overline{p\phi_{1,i}}$ and $\rho_1 U_i \overline{\phi_1 u_j}$, i.e. the interaction between pressure fluctuation and the gradient of the fluctuating fluid volume fraction (Elghobashi & Abou-Arab 1983), and the transport of momentum due to the interaction between the mean flow and fluctuations of the volume fraction and velocity. The fifth and sixth terms represent the correlation $\overline{\phi_1 u_i u_j}$, i.e. the transport of momentum due to the interaction between the fluid turbulent stresses and its volume fraction fluctuations.

The momentum equations of both phases in the radial direction can be written in a similar manner and will not be presented here.

The kinematic eddy viscosity of the carrier fluid is related to fluid turbulent kinetic energy (k) and the rate of dissipation (ϵ) of k by:

$$\nu_t = C_\mu \frac{k^2}{\epsilon}, \qquad [5]$$

where

$$C_\mu = 0.09 - 0.04f; \qquad [6]$$

$$f = 0.5R \frac{\dfrac{dU_{x,c}}{dx} - \left|\dfrac{dU_{x,c}}{dx}\right|^{0.2}}{U_{x,c} - U_{x,\infty}}. \qquad [7]$$

$U_{x,c}$ and $U_{x,\infty}$ are the axial velocities of the fluid at the jet centerline and the ambient stream respectively, R is the local jet width (Launder *et al.* 1972).

The quantities F and ν_p are evaluated in the following section.

3.2 *The momentum exchange coefficient F*

The momentum exchange coefficient F is given by

$$F = 18Z\mu_1/d^2, \qquad [8]$$

where d is the particle diameter, μ_1 is the dynamic viscosity of the fluid, and Z is a correction factor of the Stokes' drag law which depends on the particle Reynolds number and can be obtained from the standard drag curve of steady flow around a sphere (Clift *et al.* 1978) as follows

$$Z = 1 + 0.1315R_e^{(0.82-0.05\log_{10}\mathrm{Re})},\ 0.01 < R_e \leqslant 20;\ \text{and}$$

$$Z = 1 + 0.1935R_e^{0.6305},\ 20 < R_e \leqslant 260. \qquad [9]$$

The particle Reynolds number R_e is calculated from

$$R_e = d|\mathbf{U} - \mathbf{V}|/\nu_1, \qquad [10]$$

where $|\mathbf{U} - \mathbf{V}|$ is the magnitude of the total relative mean velocity vector between the two phases, and ν_1 is the kinematic viscosity of the fluid.

3.3 *Turbulent diffusivity of solid particles*

The turbulent diffusivity of solid particles is evaluated by introducing the particle Schmidt number σ_p defined as:

$$\sigma_p = \frac{\nu_t}{\nu_p}. \qquad [11]$$

Since solid particles do not in general follow the motion of the surrounding fluid from one point to another it is expected that σ_p will be different from unity and vary with the particle relaxation time and local turbulence quantities. Alonso (1981) reviewed the recent developments in evaluating σ_p and recommended the use of Peskin's (1971) formula

$$\frac{\nu_p}{\nu_t} = (1/\sigma_p) = 1 - (3/2)(L_L/\lambda)^2[Q^2/(Q+2)] \qquad [12]$$

where

$$Q = (2\rho_2/FT_L), \qquad [13]$$

and T_L and L_L are the local Lagrangian integral time and length scales respectively and λ is the Eulerian microscale.

When (L_L/λ) is much less than unity the fluid elements in the neighborhood of the solid particle will have similar velocities (i.e. homogeneous flow). Consequently, the correlation of fluid velocities encountered by the particle will be similar to the Lagrangian fluid correlation and σ_p, from [12], will approach unity. On the other hand as L_L becomes larger than λ the particle will be surrounded by random fluid velocities and its diffusivity will decrease relative to that of the fluid.

The local Lagrangian integral time scale, T_L, is evaluated assuming isotropic turbulence (Calabrese & Middleman 1979); thus

$$\epsilon = 15\nu_1\overline{u^2}/\lambda^2 \text{ and } \lambda^2 = 24\nu_1 T_L \text{ which give}$$

$$T_L = (5/12)k/\epsilon. \qquad [14]$$

The local Lagrangian length scale, L_L, appearing in [12], and the Eulerian microscale λ are calculated from

$$L_L = \sqrt{\frac{2}{3}kT_L}, \qquad [15]$$

$$\lambda = \sqrt{10\nu_1 k/\epsilon}. \qquad [16]$$

Equation [12] with the aid of [13]–[16] produces unrealistic (negative) values for the ratio of the particle diffusivity to that of the fluid. This may be attributed to the large slip

velocity between the two phases that has been neglected in Peskin's work. Soo (1967) reported the same inconsistency between the measurements and the numerical results produced by Peskin's formula for a turbulent pipe flow seeded with glass particles. He found that the half duct diameter should replace λ, in [12], to obtain good agreement with his experimental data. In the present work a parametric study optimized the length scale ratio that produces agreement with the experimental data. It was found that the ratio L_L/λ should be replaced by L_ϵ/R where R is the local width of the jet. The dissipation length scale, L_ϵ, is calculated from

$$L_\epsilon = c_\mu^{3/4} k^{3/2}/\epsilon. \qquad [17]$$

3.4 *The turbulence model*

The turbulence kinetic equation (k) of the carrier fluid is

$$\rho_1\Phi_1 U_x k_{,x} + \rho_1\Phi_1 U_r k_{,r} = \rho_1\Phi_1 \nu_t U_{x,r} U_{x,r} - \frac{4}{3}\rho_1 c_{\phi 5}\frac{\nu_t}{c_\mu}\left(\frac{\nu_t}{\sigma_\phi}\Phi_{1,r}\right)_{,r} U_{r,r}$$

Convection — Production — Extra Production

$$+ \rho_1 c_{\phi 5}\left(\frac{k}{\epsilon}\right)\nu_t\left(\frac{\nu_t}{\sigma_\phi}\Phi_{1,r}\right)_{,r} U_{x,r}U_{x,r}$$

Extra Production

$$- F\Phi_2 k\left[1 - \int_0^\infty \left(\frac{\Omega_1 - \Omega_R}{\Omega_2}\right) f(\omega)\,d\omega\right] - F(U_r - V_r)\left(\frac{\nu_t}{\sigma_\phi}\Phi_{1,r}\right)$$

Extra Dissipation

$$+ c_{\phi 5}\left(\frac{\nu_t}{c_\mu}\right) F\left[1 - \int_0^\infty \left(\frac{\Omega_1 - \Omega_R}{\Omega_2}\right) f(\omega)\,d\omega\right]\left(\frac{\nu_p}{\sigma_\phi}\Phi_{1,r}\right)_{,r}$$

Extra Dissipation

$$+ \rho_1\Phi_1\frac{1}{r}\left(\frac{\nu_t}{\sigma_k} r k_{,r}\right)_{,r} - \rho_1\Phi_1\epsilon.$$

Turbulent Diffusion — Dissipation [18]

The turbulence energy dissipation rate equation (ϵ) is

$$\rho_1\Phi_1 U_x\epsilon_{,x} + \rho_1\Phi_1 U_r\epsilon_{,r} = c_{\epsilon 1}\frac{\epsilon}{k}\left[\rho_1\Phi_1\nu_t U_{x,r}U_{x,r} + \frac{4}{3}\rho_1 c_{\phi 5}\left(\frac{\nu_t}{c_\mu}\right)\left(\frac{\nu_t}{\sigma_\phi}\Phi_{1,r}\right)U_{r,r}\right.$$

Convection — Total Production

$$\left. - \rho_1 c_{\phi 5}\left(\frac{k}{\epsilon}\right)\nu_t\left(\frac{\nu_t}{\sigma_\phi}\Phi_{1,r}\right)_{,r} U_{x,r}U_{x,r}\right] - c_{\epsilon 3}\frac{\epsilon}{k}\left[F\Phi_2 k\left(1 - \int_0^\infty \left(\frac{\Omega_1 - \Omega_R}{\Omega_2}\right) f(\omega)\,d\omega\right)\right.$$

Extra Dissipation

$$\left. + F(U_r - V_r)\left(\frac{\nu_t}{\sigma_\phi}\Phi_{1,r}\right) - c_{\phi 5}\left(\frac{\nu_t}{c_\mu}\right) F\left(1 - \int_0^\infty \left(\frac{\Omega_1 - \Omega_R}{\Omega_2}\right) f(\omega)\,d\omega\right)\left(\frac{\nu_p}{\sigma_\phi}\Phi_{1,r}\right)_{,r}\right]$$

$$+ \rho_1\Phi_1\frac{1}{r}\left(\frac{\nu_t}{\sigma_\epsilon} r\epsilon_{,r}\right)_{,r} - c_{\epsilon 2}\frac{\epsilon}{k}(\rho_1\Phi_1\epsilon). \qquad [19]$$

Turbulent Diffusion — Dissipation

The terms, in [18] and [19], involving integration in the frequency domain (ω) represent additional dissipation of k or ϵ due to the slip between the particles and the fluid and depend on the magnitude of correlation between their respective instantaneous velocities. Details of the derivation of these terms are given in (Elghobashi & Abou-Arab 1983).

The Lagrangian frequency function, $f(\omega)$ is in general affected by the presence of the dispersed phase. In the low frequency range (inertial subrange), the modulation of the Lagrangian frequency function of the carrier fluid by the dispersed phase can be neglected (Al Taweel & Landau 1977). Thus in the present work the Lagrangian frequency function is given by (Hinze 1975),

$$f(\omega) = \left(\frac{2}{\pi}\right)\left(\frac{T_L}{1+\omega^2 T_L^2}\right), \qquad [20]$$

where ω ranges from 1 to 10^4 ($\sec^{-1}$) and T_L is calculated from [14]. It should be mentioned that the above expression[20] for $f(\omega)$ is different from the one employed by Elghobashi & Abou-Arab (1983). The former is simpler to use than the latter which contained an exponential. However, in order to produce identical results by both forms, the coefficient $c_{\epsilon 3}$ appearing in [19] must be lowered from 1.2 to 1.0 (see table 2). The functions Ω_1, Ω_2, Ω_R, α and β are evaluated according to (Elghobashi & Abou-Arab 1983) from

$$\Omega_1 = \left(\frac{\omega}{\alpha}\right)^2 + \sqrt{(6)}\left(\frac{\omega}{\alpha}\right)^{3/2} + 3\left(\frac{\omega}{\alpha}\right) + \sqrt{(6)}\left(\frac{\omega}{\alpha}\right)^{1/2};$$

$$\Omega_2 = \beta^{-2}\left(\frac{\omega}{\alpha}\right)^2 + \sqrt{(6)}\beta^{-1}\left(\frac{\omega}{\alpha}\right)^{3/2} + 3\left(\frac{\omega}{\alpha}\right) + \sqrt{(6)}\left(\frac{\omega}{\alpha}\right)^{1/2};$$

$$\Omega_R = [(1-\beta)\omega/(\alpha\beta)]^2;$$

$$\alpha = 12\nu_1/d^2,$$

$$\beta = 3\rho_1/(2\rho_2 + \rho_1). \qquad [21]$$

The values of the coefficients appearing in [18] and [19] are listed in table 2 below.

Table 2. Coefficients of the turbulence model

σ_ϕ	σ_k	c_μ	σ_ϵ	$c_{\phi 5}$	$c_{\epsilon 1}$	$c_{\epsilon 2}$	$c_{\epsilon 3}$
1	1	[6]	1.3	0.1	1.44	[22]	1.0

The constant $c_{\epsilon 2}$ in table (2) is given by

$$c_{\epsilon 2} = 1.92 - 0.0667f \qquad [22]$$

where f is given by [7].

It is seen that three new coefficients (σ_ϕ, $c_{\phi 5}$, $c_{\epsilon 3}$) are now added to the well-established $k-\epsilon$ coefficients for single-phase flows, namely σ_k, σ_ϵ, c_μ, $c_{\epsilon 1}$ and $c_{\epsilon 2}$. The values of the new coefficients have been optimized to produce good agreement with the data of (Moderress *et al.* 1982, 1983) for one particle size (200 μm) and then used to predict the data of the other size (50 μm). It should be emphasized that more validation testing is required to establish the universality of these coefficients.

3.5 *Boundary conditions*

The parabolic flow considered here requires the prescription of three boundary conditions for each dependent variable. Table 1 provides these conditions at the pipe exit plane and at the jet boundary. At the axis of symmetry ($r = 0$) all the radial gradients are set to zero, in addition to the vanishing radial velocity of each phase.

4. NUMERICAL SOLUTION PROCEDURE

The marching finite-difference procedure employed in this work is a modified version of that developed and described by Spalding (1979) for laminar two-phase flows. The modifications included the treatment of the turbulent correlations existing in the continuity and momentum equations of the two-phases. Only a brief outline is given here.

The coordinates of the expanding finite-difference grid are x and ψ, the stream function based on the mean gas-phase properties, i.e.

$$\psi = \int_0^r \rho_1 \Phi_1 U_x r \, dr. \qquad [23]$$

The steps followed to obtain the solution at a given axial location are:

(1) Guess the downstream Φ_1^* distribution.

(2) Solve for U_x downstream.

(3) Solve for k and ϵ; obtain r's and solve for U_r.

(4) Obtain $p(r)$ from U_r equation.

(5) Solve for downstream V_x, V_r, Φ_2 and get Φ_1.

(6) Compare the new Φ_1 with the guessed Φ_1^* and repeat steps 1–5 until the solution converges before marching to the next station.

It was found that 3 iterations are needed at each station to achieve convergence.

5. RESULTS AND DISCUSSIONS

The results presented here were obtained using 40 lateral nodes to span the flow domain between the centerline of the jet and its outer edge. Grid-dependence tests were conducted with 30, 40 and 50 lateral nodes and different axial step sizes and concluded that the 40 node grid results are virtually grid-independent.

In what follows we compare the predicted with the measured distributions of the mean velocities, volume fractions of the two phases, turbulence intensity and shear stress of the gaseous phase and the jet spreading rate.

Figure 2 shows the radial profiles of the mean axial velocities of the two phases at $x/D = 20$, normalized by the centerline velocity of the single-phase jet, $U_{c,S,ph}$. The flow conditions are those of case 3 in table 1. Also shown is the mean velocity profile of the turbulent single-phase jet having the same Reynolds number (14100) at the pipe exit.

It is seen that the centerline velocity of the dispersed phase is about 1.8 times that of the carrier fluid although the latter is 1.3 times the former at the pipe exit. This can be explained by the fact that large-diameter ($> 10\mu$) particles do not respond well to the fluid turbulent fluctuations ([7] and [8] indicate that for a fixed ρ_2 and T_L we get $\nu_p \ll \nu_t$ for small F, i.e. large d) thus the main force that accelerates a particle in the radial direction is the viscous drag exerted on the particle by the fluid radial velocity, U_r. Now this drag force is proportional to $(U_r - V_r)$ and since U_r is negative in the outer region of the jet (and $V_r < U_r$) the resulting force will be directed inwards thus limiting the radial spread of the particles. This is evident in figure 3 where the concentration of the solid particles vanish at a radial distance of $r/x \simeq 0.12$ while the fluid spreads to at least three times this distance. Conservation of momentum of each phase then results in the solid-phase axial velocity

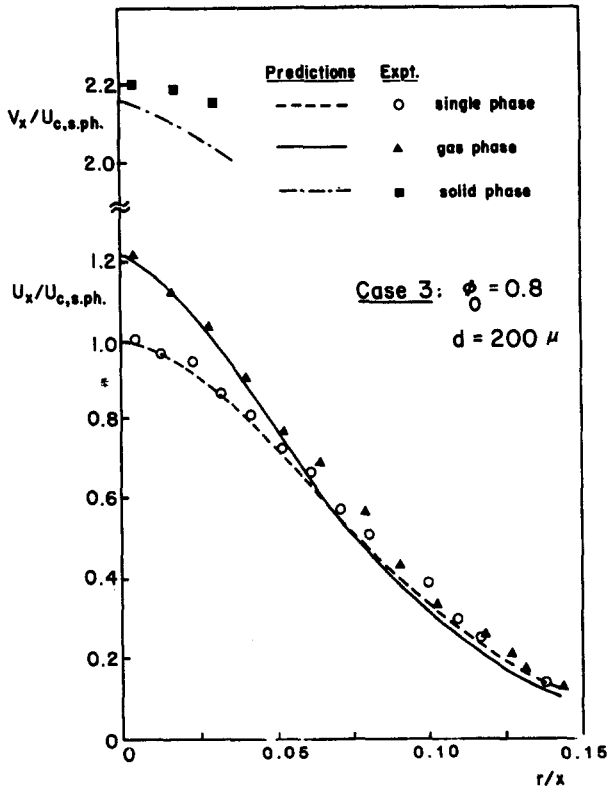

Figure 2. Mean velocity profiles at $x/D = 20$ for case 3.

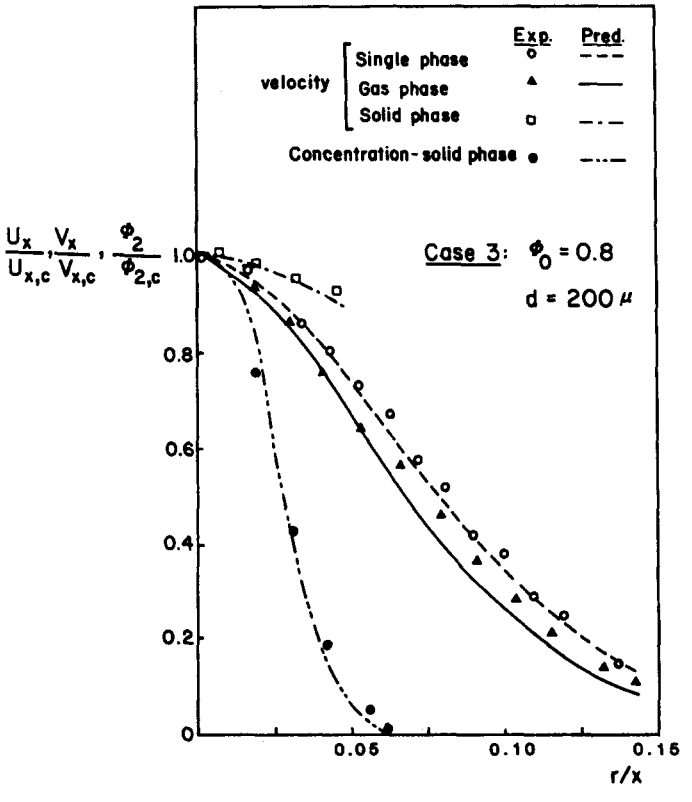

Figure 3. Normalized mean velocity and volume fraction profiles at $x/D = 20$ for case 3.

being much higher than that of the fluid, and in turn the particles continue to be a source of momentum for the fluid. It is also clear from figure 3 that the single-phase jet is wider than the particle-laden jet; this will be discussed later in this section. Both figures 2 and 3 display in general good agreement between the measured and predicted velocity and concentration profiles.

The measured and predicted mean velocity profiles for case 2 ($d = 50\,\mu$, $\Phi_0 = 0.85$, Re = 13300) are shown in figure 4. Similar qualitative behavior to that of case 3 is exhibited here except that now the ratio between the experimental velocities of the solid and the fluid is only about 1.15 instead of 1.8 in case 3 ($d = 200\,\mu$, $\Phi_0 = 0.8$, Re = 14100). The main difference between the two cases is the particle diameter, and thus any quantitative change in the mean velocity profiles is attributed to the interphase surface area acted on by the viscous drag. This surface area in case 2 is four times that in case 3, since, for nearly the same loading ratio, the number of the 50 μ particles is 64 times that of the 200 μ particles. This increase in the number of particles and interphase area results in augmenting the momentum sources of the carrier fluid thus reducing the rate of decay of its centerline velocity.

The agreement is very good between the measured and predicted fluid velocity while the solid-phase velocity is underestimated by 8% in the inner region, a discrepancy well within the bounds of experimental error. Figure 5 shows the mean velocity profiles at $x/D = 20$ for case 1 (50 μ, Re = 13300, $\Phi_0 = 0.32$) which has a lower loading ratio, Φ_0, than case 2, otherwise the two cases are identical. Again the behavior of the two phases is similar to that observed in the other two cases except that now the experimental ratio between

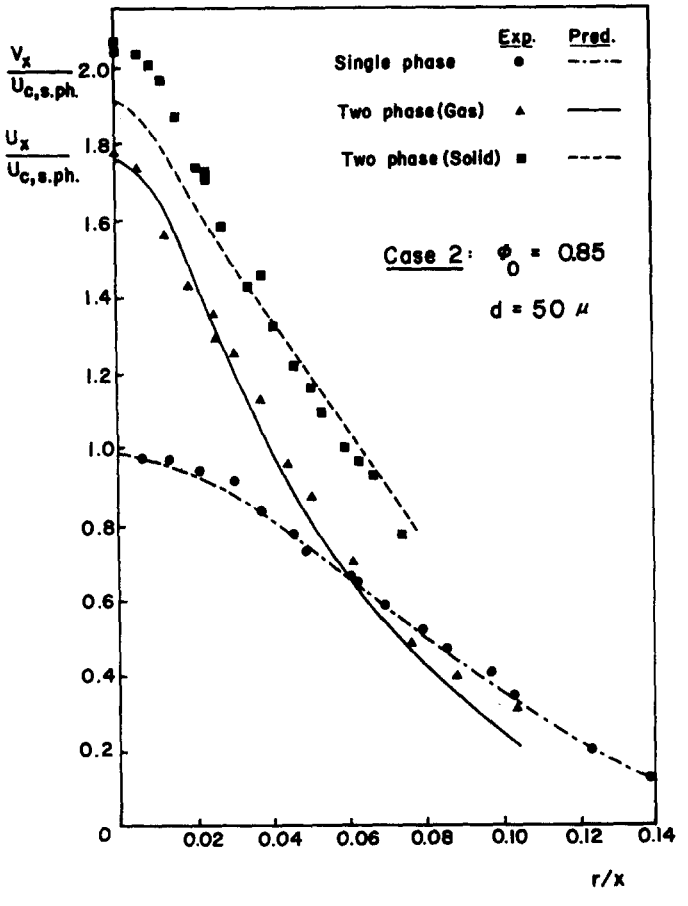

Figure 4. Mean velocity profiles at $x/D = 20$ for case 2.

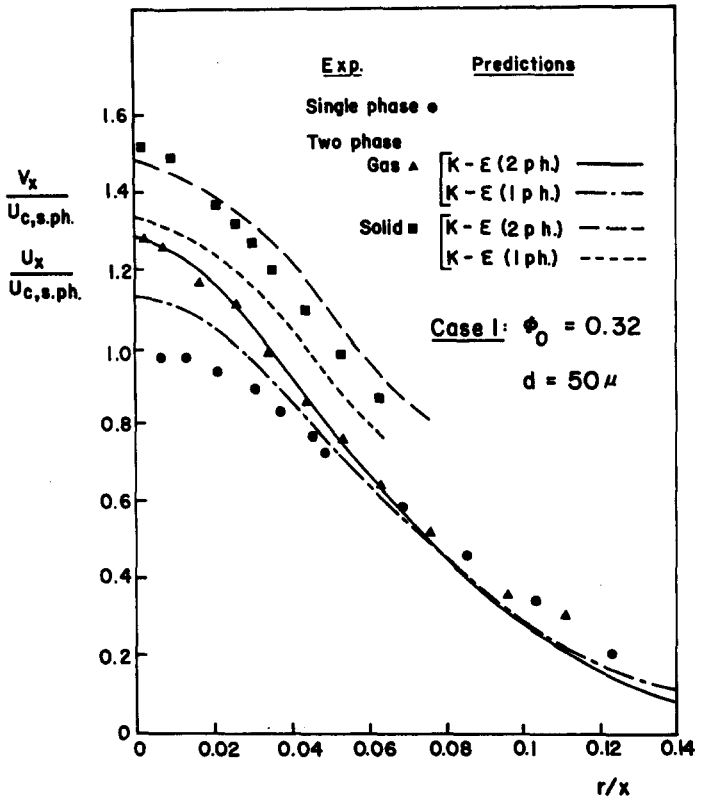

Figure 5. Mean velocity profiles at $x/D = 20$ for case 1.

the centerline velocities of the solid and the fluid is 1.2 instead of 1.15 in the higher-loading case (case 2). This indicates that, other conditions being the same, higher loading reduces the rate of decay of the fluid centerline velocity. This is a result of the increase in the number of particles and hence their contribution to the fluid momentum as discussed earlier.

In order to distinguish between the dispersed phase effects on the mean motion (inertia and drag) and on turbulence (diffusion) we show (figure 5) the mean velocity profiles

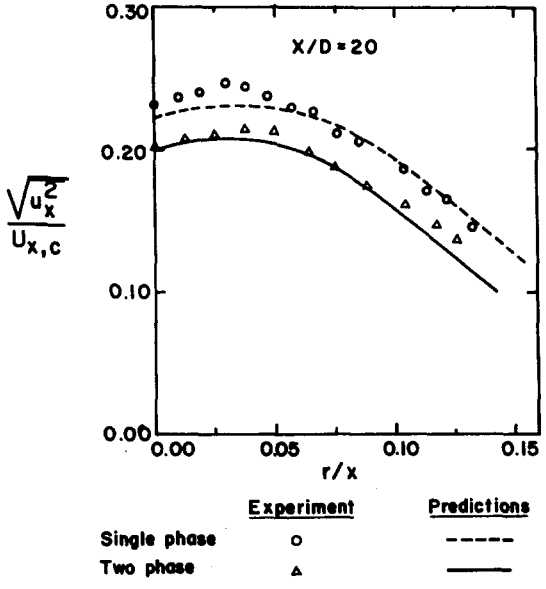

Figure 6. Turbulence intensity profile at $x/D = 20$ for case 3.

obtained by solving the complete two-phase momentum equations [1], [2] together with the single-phase k and ϵ equations (i.e. [3], [4] without the additional production and dissipation terms due to the dispersed phase). We see that the resulting *increase* in the fluid centerline velocity, as compared to that of the single-phase jet, is only *half* that measured and predicted by the new $k - \in$ model. Stated differently, the modulation of the fluid mean-velocity profile by the dispersed phase is not only due to the particles inertia and drag but equally important due to the additional turbulence dissipation. This in turn reduces the fluid momentum diffusivity with the result of a peaked velocity profile near the jet centerline. The additional turbulence dissipation is caused mainly by the fluctuating particle relative velocity and its correlation with the fluid velocity fluctuation[6]. The consequent reduction in the fluid turbulence intensity and shear stress is displayed in figures 6 and 7 where the agreement between the measurement and prediction is good.

Figure 8 shows the effect of the dispersed phase on the spreading rate of the jet by comparing the different $Y_{1/2} \sim x$ distributions of the three cases, where $Y_{1/2}$ is the radius at which the fluid mean axial velocity is half that at the centerline. While for a turbulent single-phase jet the value of the slope $(dY_{1/2}/dx)$ is constant ($\simeq 0.08$), that for a two-phase jet is a function of the dispersed phase properties such as particle diameter and density and loading ratio. This dependence is displayed in the figure. For case 3 ($d = 200\mu$, $\Phi_0 = 0.8$) the predicted slope value is 0.053, for case 2 ($d = 50\mu$, $\Phi_0 = 0.85$) it is 0.046, and for case 1 ($d = 50\mu$, $\Phi_0 = 0.32$) it is 0.064. Cases 3 and 2 have nearly the same loading ratio but the particle diameter in the latter is one quarter that of the former; the result being a reduction of the spreading rate by more than 13%.

Cases 1 and 2 are identical except that the loading ratio in the latter is 2.66 times that of the former; the result being a reduction of the spreading rate by 28%.

The figure also shows the discrepancy that results in predicting the spreading rate if the single-phase $k - \epsilon$ model is used instead of the proposed model. The former predicts for case 1 a slope of 0.072 while the latter agrees with the experimental value of 0.064.

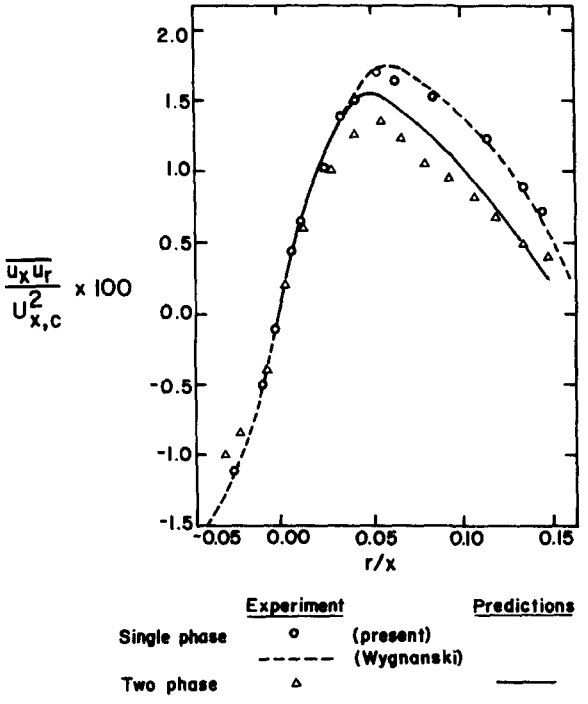

Figure 7. Turbulence shears stress profile at $x/D = 20$ for case 3.

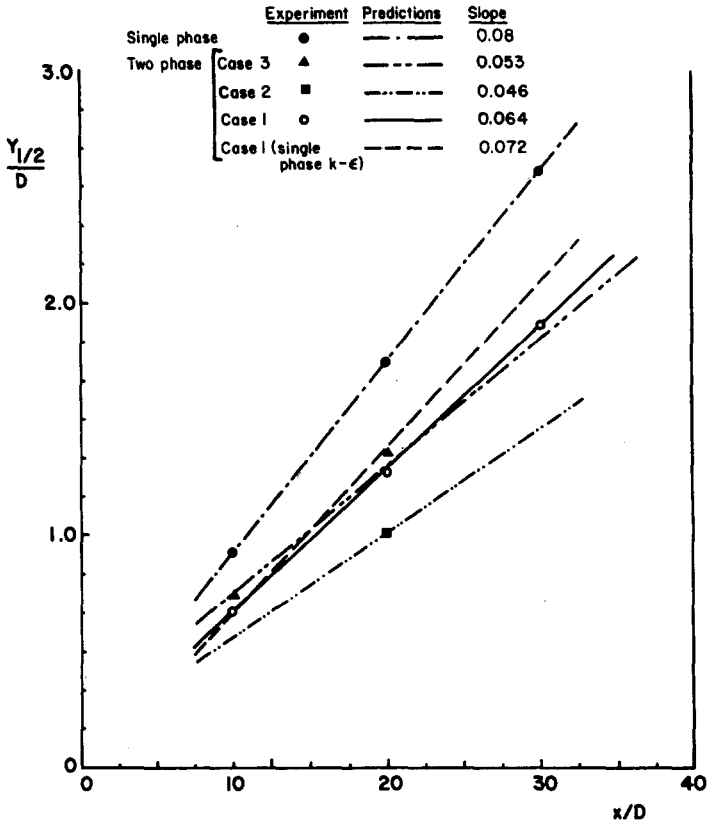

Figure 8. Jet spread rates for the three cases.

As explained earlier this is due to the fact that the additional dissipation of turbulence energy due to the dispersed phase is accounted for in the proposed model.

6. CONCLUDING REMARKS

It has been shown that the turbulence model, introduced by (Elghobashi & Abou-Arab 1983), allows the correct simulation of the two-phase turbulent jet.

The additional dissipation produced by the relative velocity fluctuations has a significant effect on the jet development. Further testing is needed to check the universality of the coefficients in the model.

Acknowledgements—This work has been supported by a U.S. Department of Energy grant No. DEFG22-80PPC-30303 and NASA grant No. NAG3-176. The authors express their thanks to Mrs. Verna Bruce for her expert typing of the manuscript.

REFERENCES

AL TAWEEL, A. M. & LANDAU, J. 1977 Turbulence modulation in two-phase jets. *Int. J. Multiphase Flow* **3**, 341–351.

ALONSO, C. V. 1981 Stochastic models of suspended sediment dispersion. *A.S.C.E.* **107**, 733–757.

BARKER, S. 1973 Laser–Doppler measurements on a round turbulent jet in dilute polymer solutions. *J. Fluid Mech.* **60**, 721–731.

CALABRESE, R. V. & MIDDLEMAN, S. 1979, The dispersion of discrete particles in a turbulent fluid field. *AIChE* **25**, 1025–1035.

CLIFT, R., GRACE, J. R. & WEBER, M. E. 1978 *Bubbles, Drops and Particles.* Academic Press, New York.

ELGHOBASHI, S. & ABOU-ARAB, T. W. 1983 A two-equation turbulence model for two-phase flows. *Phys. Fluids* **26**, 931–938.

HETSRONI, G. & SOKOLOV, M. 1971 Distribution of mass, velocity, and intensity of turbulence in a two-phase turbulent jet. *J. Appl. Mech.* **33**, 315–327.

HINZE, J. O. 1975 *Turbulence.* McGraw-Hill, New York.

LAUNDER, B. E., MORSE, A., RODI, W. & SPALDING, D. B. 1972 The prediction of free shear flows—a comparison of the performance of six turbulence models. TM/TN/19. Imperial College, London.

MODARRESS, D., WUERER, J. & ELGHOBASHI, S. 1982 An experimental study of a turbulent round two-phase jet. *AIAA/ASME 3rd Joint Thermophysics, Fluids, Plasma and Heat Transfer Conf.* St. Louis, Missouri.

MODARRESS, D., TAN, H. & ELGHOBASHI, S. 1983 Two-component LDA measurement in a two-phase turbulent jet. *AIAA 21st Aerospace Sci. Meeting.* Reno, Nevada.

PESKIN, R. L. 1971 Stochastic estimation applications to turbulent diffusion. *Int. Symp. on Stochastic Diffusion* (Edited by C. L. CHIU), p. 251. University of Pittsburgh, Pennsylvania.

POPPER, J., ABUAF, N. & HETSRONI, G. 1974 Velocity measurements in a two-phase turbulent jet. *Int. J. Multiphase Flow* **1**, 715–725.

SOO, S. L., 1967, *Fluid Dynamics of Multiphase Systems*, p. 59. Blaisdell, Waltham, Mass.

SPALDING, D. B., 1979, *Numerical Computation of Multiphase Flows.* Lecture Notes, Thermal Sciences and Propulsion Center, Purdue University, Indiana.